KEK Report 91-10
December 1991
A

Analysis of the Prebuncher for the KEK 40-MeV Proton Linac

Takao KATO

NATIONAL LABORATORY FOR
HIGH ENERGY PHYSICS

KEK Reports are available from:

Technical Information & Library
National Laboratory for High Energy Physics
1-1 Oho, Tsukuba-shi
Ibaraki-ken, 305
JAPAN

Phone: 0298-64-1171
Telex: 3652-534 (Domestic)
(0)3652-534 (International)
Fax: 0298-64-4604
Cable: KEKOHO

ANALYSIS OF THE PREBUNCHER FOR THE KEK 40-MeV PROTON LINAC

Takao KATO

KEK, National Laboratory for High Energy Physics
Oho 1-1, Tsukuba-shi, Ibaraki-ken, 305, Japan

Abstract

The electromagnetic fields of the prebuncher for the KEK 40-MeV proton linac have been studied using the code MAFIA. Part of the calculated results were compared with the experimental results. A beam simulation of the beam transport line between the prebuncher and the linac was performed using code LEBT; it runs on a supercomputer in order to calculate beam dynamics, including space-charge effects. The capture efficiency of the linac and the emittance growth in the beam line are discussed in connection with the space-charge effects.

KEYWORDS: prebuncher, proton linac, capture efficiency, emittance growth, space-charge effects, supercomputer

1. Introduction

A single-prebuncher system has been operated for the KEK 40-MeV proton linac (DTL) since 1974. The capture efficiency of the linac was increased from 25 to 50% using the prebuncher system[1] for a high-intensity proton beam of more than 200 mA. The capture efficiency was increased up to 60% after changing the accelerating beam from protons to low-intensity negative hydrogens in 1985. Two computer codes suitable for analyzing the operation of the prebuncher system were recently obtained. One, called MAFIA,[2] calculates the rf properties for a three-dimensional geometry. The other, called LEBT, was written by the author; it runs on a supercomputer in order to calculate beam dynamics, including space-charge effects. This paper deals with both an analysis of the electromagnetic fields of the prebuncher using MAFIA and a beam dynamics simulation using LEBT. The capture efficiency of the linac and the emittance growth in the beam line are discussed in connection with the space-charge effects on the basis of both the calculated and experimental results.

2. Structure of the prebuncher

The 201-MHz prebuncher is similar in design to that used at both Rutherford Laboratory and BNL.[3] The cavity is a coaxial $\lambda/2$ resonator (Figs. 1 and 2); λ is the wavelength of the cavity. The cavity length (583 mm) is 163 mm shorter than the half-wavelength of the resonant frequency, due to two capacitive accelerating gaps in the center part of the cavity. The two accelerating gaps are spaced 89 mm apart. Thus, a 750-keV proton travels through the distance

within 1.5-times the rf period. Since the accelerating electric fields in the gaps point in opposite directions, a proton is accelerated in the gaps with the same rf phase. The center part of the cavity is regarded as being a two-cell drift tube linac which has a drift tube and two half-drift tubes on both end plates. The beam-hole radius (18 mm) is too large from the viewpoint of uniformity of the field distribution within the gap. Therefore, drift tubes have been installed with grid-rings for the purpose of improving the gap fields. However, it is not sufficiently large from the viewpoint of beam losses, since the beam radius is 17 mm for a normalized beam emittance of 3πmm·mrad.

3. Calculation of the electromagnetic fields in the prebuncher

Code MAFIA calculates the rf properties of the prebuncher. The number of meshes used in the calculation was 159695 (41x41x95), resulting in a calculation time of 89 minutes for ten resonant modes on an HITAC M680 computer. At first, the calculation was performed for a structure that did not have grid-rings (no-grid-rings prebuncher). Figures 3 and 4 show the calculated electric field distribution in the zx-plane and the calculated magnetic field distribution in the yz-plane for the fundamental mode. The calculated electric fields (E_z) along the z-axis are plotted in Figs.5 and 6. The fields have been normalized by the maximum value along the z-axis. It can be seen that a tail of the fields enters the beam-hole of the drift tubes to a large extent, thus decreasing the transit-time factors. Table 1 summarizes the calculated average accelerating fields (E_0) and the transit-time factors (T) for three

kinds of field distributions given in Fig.5. The effective accelerating field (E_0T) along an axis 12 mm away from the z-axis is larger than that along the z-axis by 47%. It is expected that the above-mentioned fact deteriorates the efficiency of the prebuncher system, since the buncher voltage for an off-axis particle is not sufficiently large for making the desirable bunch.

The off-axis transit-time factor is given by[4]

$$T(r) = T(0)\, I_0(kr), \quad I_0(x) = 1 + \frac{x^2}{4} + \frac{x^4}{64} + \text{- - -},$$

where T(0) is an on-axis transit-time factor, r is the distance from the z-axis, $I_0(x)$ is a modified Bessel function, $k=\beta\lambda/2\pi$, $\beta=v/c$, v is the velocity of a particle, and c is the velocity of light. The above formula gives a T(r)/T(0) of 1.07 and 1.43 for r of 5 and 12 mm, respectively. The good agreement between the calculated and theoretical values shows the excellent accuracy of calculations using MAFIA.

The original design of the prebuncher uses four grid-rings (Fig.1) in order to improve the field distribution. Figure 7-1 shows a grid-ring shape used for the prebuncher. In the calculation, the shapes of the rods in Fig.7-1 are modified because of a limitation in the available minimum mesh size in the code. The modified grid-ring shape is shown in Fig.7-2. The calculated electric fields (E_z) along the z-axis are plotted in Fig.8. Figure 9 shows the calculated electric fields (E_z) in the xy-plane at the gap center. There have been excellent improvements in the use of the grid-rings. First, the tail of the field into the beam-hole of the drift tubes becomes small, resulting in an increase in transit-time factors. Secondly, the uniformity of the field distribution in the xy-plane is greatly

improved. Table 2 summarizes the accelerating parameters for three kinds of field distributions. The grid-rings cause a slight beam loss of about 10% due to scattering.[1]

Figure 10 shows the calculated electric field (E_y) along an axis separated from the z-axis by 12 mm. The calculation was performed using the no-grid-rings structure. Since the E_y-field (also E_x) changes sign at the midpoint of the gap, a stable particle that gains no acceleration or deceleration in the z-direction is deflected by the E_y-field. (A particle away from 90 degrees from the stable one is not deflected.) Therefore, theses deflecting fields cause emittance growth in the prebuncher. The grid-rings improve the deflecting field, as can be seen in Fig.11.

4. Measurement of the electric field in the prebuncher

The electric field in the no-grid-rings prebuncher was measured[5] using a bead perturbation method. Figure 12 shows a typical electric field measured along the z-axis. The average electric fields and transit-time factors calculated from the measured field are summarized in Table 3. The fields were normalized by the maximum value obtained in the two gaps. The measured transit-time factors agree with the calculated values within the experimental accuracy determined from the uncertainty of the bead position and the fluctuation of the base line of the signal. The calculated maximum accelerating field along an axis at r=12 mm is larger than that along the z-axis by 62% (Fig.5), while the measurement gives 58% under similar conditions.

5. Code LEBT for beam transport simulation with space-charge

The equations of motion for a particle of charge q in a beam transport line are given by

$$\frac{d\mathbf{p}}{dt} = q\,(\,\mathbf{E} + \mathbf{v} \times \mathbf{B}\,)\ ,$$

$$\mathbf{p} = m_0 \gamma\, \mathbf{v}\ ,\ \gamma = 1 / \sqrt{1 - \beta^2}\ ,$$

and

$$v^2 = v_x^2 + v_y^2 + v_z^2\ ,$$

where **p** is the momentum of the particle, **E** is the electric field, **B** is the magnetic field of the focusing elements, and m_0 is a rest mass. The space-charge force on the i-th particle is written as

$$\mathbf{E}_i = \frac{q}{4\pi\varepsilon_0} \sum_{j \neq i} \frac{1}{r_{ij}^2}\ ,$$

where ε_0 is the permittivity of free space and $\mathbf{r}_{ij}$ is the distance between the i-th and j-th particles. The second-order differential equation mentioned above is solved numerically by the Runge-Kutta method of fourth order. The main part of the code, including a calculation of the space-charge forces among all particles, is vectorized in order to run on a supercomputer (HITAC S820/80). A vectorized ratio of above 99.7% is obtained, resulting in a calculation speed rate more than thirty-times as fast as that with a scalar computer (HITAC M-680H). The accuracy of the solution has been confirmed by comparing the results of the code with those by the transfer matrix method for zero current as a function of a time interval. This procedure is also used for determining the optimum interval. Six-dimensional particle data are written in the external file

during the calculation, which is used both for finding macroscopic properties of the bunch and for graphic representations on the scalar computer.

6. Beam simulation for the prebuncher system with code LEBT

Figure 13 shows the beam transport line between the prebuncher and the linac. Figure 14 shows the β-functions of the line calculated from the focusing magnet parameters[6] for the latest operation. Injection particles of K-V distribution with a 100% normalized emittance of 3 πmm·mrad, an energy width of zero, and a phase width of 360 degrees, are used for the simulation. Twiss parameters of the transverse emittances for a zero current beam are chosen so that a matched beam may be obtained at the DTL entrance. In the calculation, a virtual gap at the center of the two gaps is substituted for the two gaps of the prebuncher. An electric field (E_z) in the gap is a sinusoidal function of time with a uniform amplitude, both transversely and longitudinally. The capture efficiency of the linac is calculated from the longitudinal condition that the phase of the particle is inside of the longitudinal acceptance of the linac. Here, the acceptance is assumed to be constant for the beam currents. The energy width of the longitudinal acceptance of the linac is not taken into account, because it is so large that all particles are always within the energy-acceptance. It takes 400 sec to perform a simulation with 2000 particles on the supercomputer.

The capture efficiencies, thus obtained, are represented in Fig.15 as a function of the applied voltage in the gap. The capture efficiency for a 200-mA beam is lower than that for a zero-current

beam by 12%. The decrease in the capture efficiency for a 20-mA beam is negligibly small.

Figure 16 shows the calculated transverse emittance growth as a function of the beam intensity. Since there is no deflecting rf fields in the prebuncher of the simulation, the emittance growth, thus obtained, is caused by space-charge effects in connection with the bunching effects. Figure 17 shows the calculated longitudinal emittance for zero-current at the DTL entrance. Figure 18 shows similar results for a 200-mA beam. It can be seen that the space-charge force deforms the center part of the emittance shape, where the charge density increases locally because of the bunching effect. This fact results in both a decrease in the capture efficiency, due to bunch lengthening, and a change in the energy distribution. Figure 19 shows the energy distribution for three kinds of beam intensities. The kinetic energy of a particle located at the head of the bunch is lower than the average energy because of prebuncher deceleration. In addition, the space-charge electric field on the particle is in the z-direction. Thus, the kinetic energy of the particle increases during the bunching process. Figure 19-3 shows a narrow energy width caused by the process mentioned above. The optimum beam intensity that minimizes the energy width is approximately 300 mA (Fig.20) for this prebuncher system.

It is well known that there is no emittance growth if the space-charge force is linear. Although a K-V distribution is assumed for the injection particles, large nonlinear forces arise from a sudden bunching process caused by a sinusoidal prebuncher voltage. Figures 21 and 22 show the z and x-components of the electric field

arising from the space-charge (200 mA) for each particle at the DTL entrance. A linear electric field arising from the uniformly-distributed equivalent ellipsoid is also plotted as an inclined-line. The concentration of the non-linear force around the center of the bunch is clear (Fig.21). The difference between the field on a particle and that represented by the inclined-line corresponds to a nonlinear part of the field and causes emittance growth in the beam line.

7. Discussion

The calculated emittance growth varies along the z-axis (Fig.23). It can be seen that the emittance growth rate rapidly increases as bunching grows in the beam line. Therefore, much care is necessary in studying the transverse emittance growth in the linac with a bunching system by a prebuncher, since the emittance measured in front of the DTL entrance is smaller than that at the DTL entrance for a high-intensity beam.

A measurement of the emittance growth in the beam transport line between the grid-rings prebuncher and the emittance monitor located at a distance of 11.3 cm upstream from the DTL entrance was performed[7] with more than a 200-mA proton beam with a 90% normalized emittance of 4 πmm·mrad, resulting in a 13% emittance growth (for y-y' phase plane). The calculated emittance growths for a matched beam with similar beam parameters are 6% (for x-x') and 30% (for y-y'). It should be noted that the y-y' emittance for protons measured in 1977 corresponds to the x-x' emittance in the calculation for H^- beams. Therefore, the measured value is twice as large as the calculated one. It is necessary

to obtain detailed information regarding the measurement (the beam intensity, the buncher voltage and phase, and the tuning of the transverse focusing) in order to compare the experimental results with the calculation precisely.

Figure 16 shows some asymmetry in the emittance growth between two transverse phase spaces. A detailed calculation shows that the emittance growth depends on both the twiss parameters of the injection beam and the transverse beam sizes during bunching process.[8]

The accelerating beam has been changed from protons to negative hydrogens since 1985. There are two remarkable merits that improves the beam quality: one is a lower beam current, less than 20 mA; the other is a smaller transverse emittance of about a half the old value. As a result, the capture efficiency of the linac has become more than 60%. This value, however, is lower than the calculated value (75%). One of the reasons for the low capture efficiency is the unsatisfactory field distribution in the prebuncher. The grid-rings have been removed since 1985 in order to avoid beam losses by scattering. Therefore, the effective accelerating field varies as a function of the distance form the z-axis, as shown in Figs. 5 and 6 and Table 1.

Acknowledgements

The author wishes to express his gratitude to Prof. M. Kihara for valuable discussions and suggestions. He also wishes to give thanks to Prof. E. Takasaki regarding his careful reading of the manuscript.

References

1) S. Anami et al.: "Status of the KEK Injector Linac", Proc. 1979 Linear Accelerator Conf., 94, (1979), KEK-PREPRINT-79-20.
2) T. Weiland: "On the Numerical Solution of Maxwell's Equations and Applications in the Field of Accelerator Physics", Particle Accelerators, 15, 245 (1984).
3) G. W. Wheeler et al.: "The BROOKHAVEN 200-MeV Proton Linear Accelerator", Particle Accelerators, 9, 1 (1979).
4) L. Smith: "Linear Accelerators", Handbuch der Physik, Band XLIV, p.341(1959).
5) T. Kato: "RF Measurement of Prebuncher", KEK Accelerator Department Study Note, ASN-244(1985)(in Japanese).
6) A. Takagi: Private communication.
7) T. Sakaue et al.:"Change of emittance with prebuncher", KEK Accelerator Department Study Note, ASN-58 (1977)(in Japanese).
8) To be published.

Table 1 Calculated accelerating parameters for the no-grid-rings prebuncher. E_p denotes the maximum electric field along the axis.

	$E_0(r)/E_p(r)$	E_0	T	E_0T	T(r)/T(0)
r=0 mm	0.49	1.0	0.49	1.0	1.0
r=5 mm	0.49	1.0	0.52	1.06	1.06
r=12 mm	0.51	1.03	0.70	1.47	1.43

Table 2 Calculated accelerating parameters for the grid-rings prebuncher.

	E_0	T	E_0T
r=0 mm	1.0	0.91	1.0
r=5 mm	1.02	0.93	1.04
r=12 mm	1.02	0.94	1.05

Table 3 Measured electric field and transit-time factors along a beam axis for the no-grid-rings prebuncher.

	E_0/E_p	T	E_p
First gap	0.45	0.43	0.99
Second gap	0.46	0.45	1.00

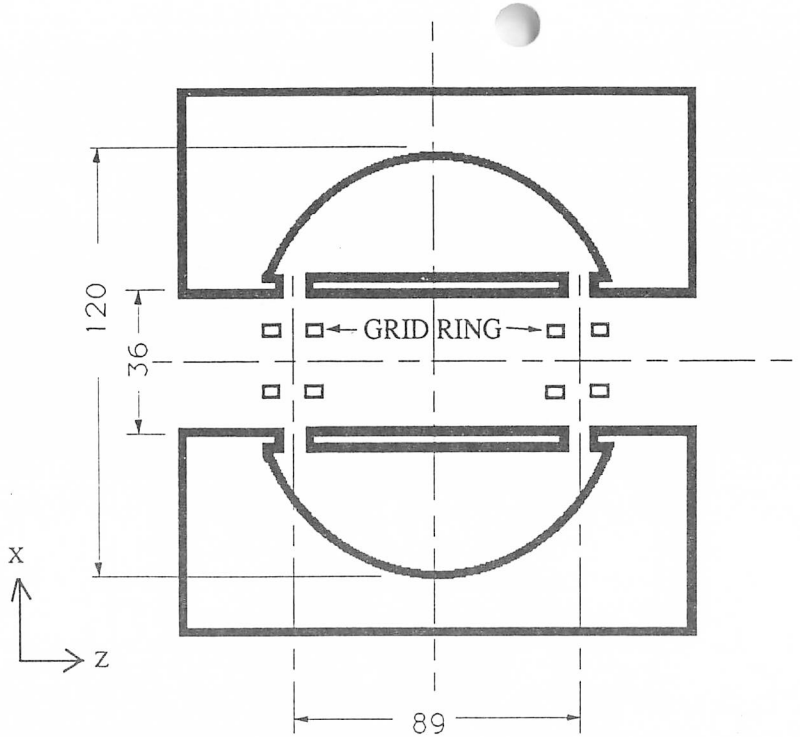

Fig. 1 Geometry of the prebuncher (side view).

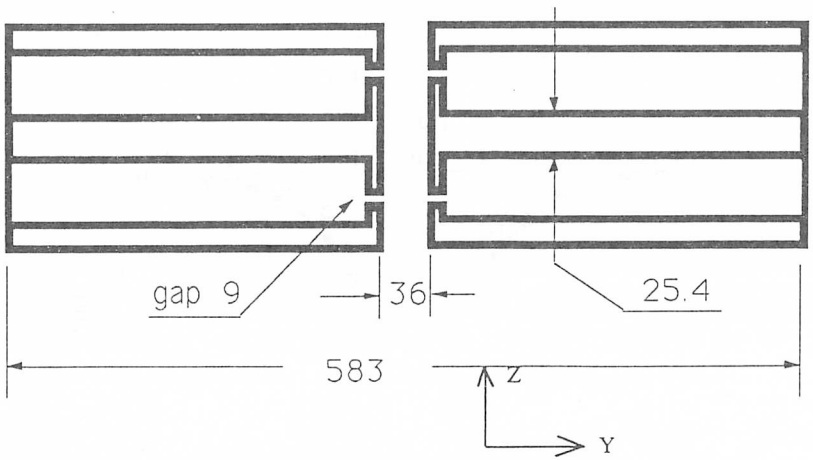

Fig. 2 Geometry of the prebuncher (top view).

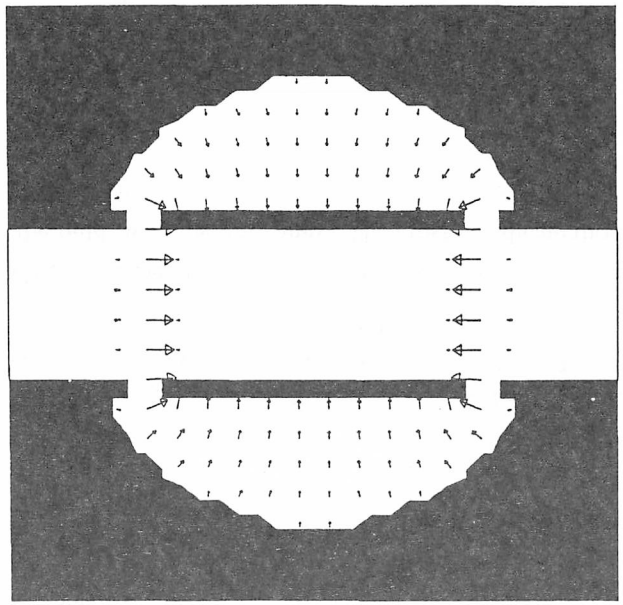

Fig. 3 Calculated electric field in the zx-plane.

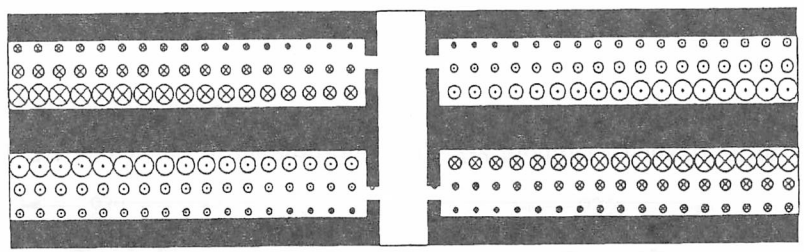

Fig.4 Calculated magnetic field in the yz-plane.

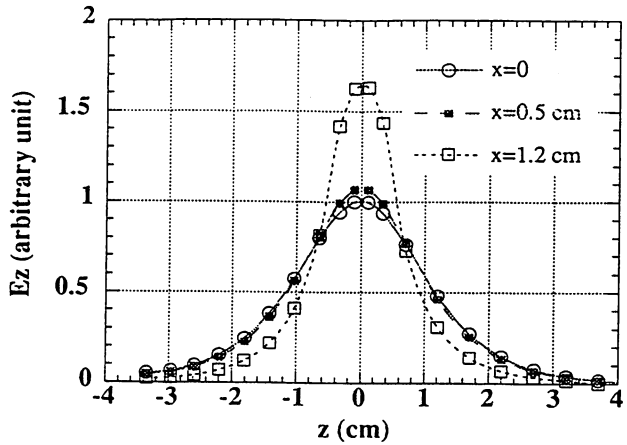

Fig. 5 Calculated electric fields Ez at y=0 for the no-grid-rings prebuncher. z=0 stands for the gap center.

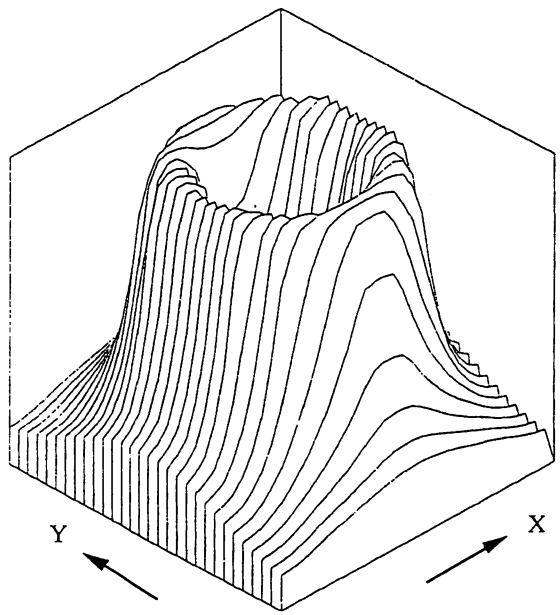

Fig. 6 Three-dimensional plot of the calculated electric fields Ez in the xy-plane at the gap center.

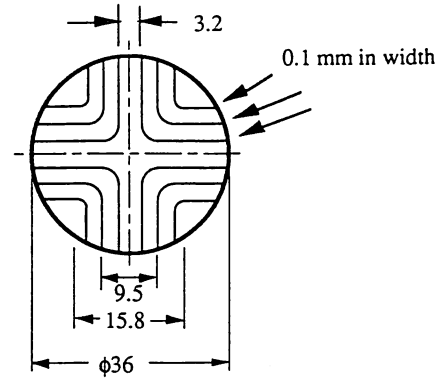

Fig. 7-1 Geometry of the grid-ring used for the prebuncher.

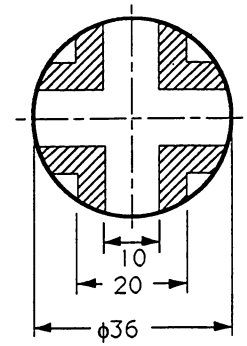

Fig. 7-2 Modified geometry of the grid-ring used for the calculation.

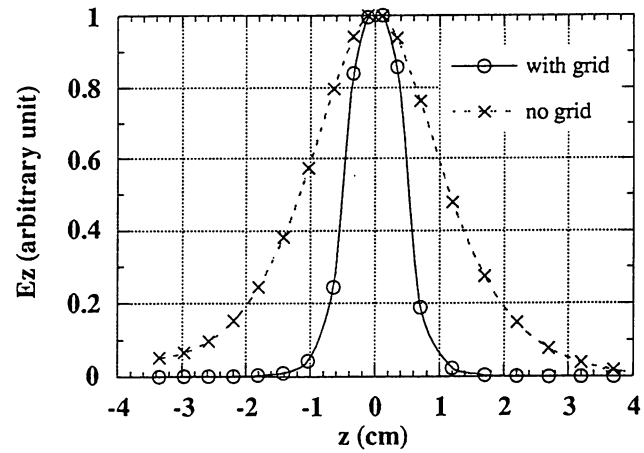

Fig. 8 Calculated electric fields along the z-axis. The circles indicate the fields with the grid-rings. The crosses indicate those without the grid-rings.

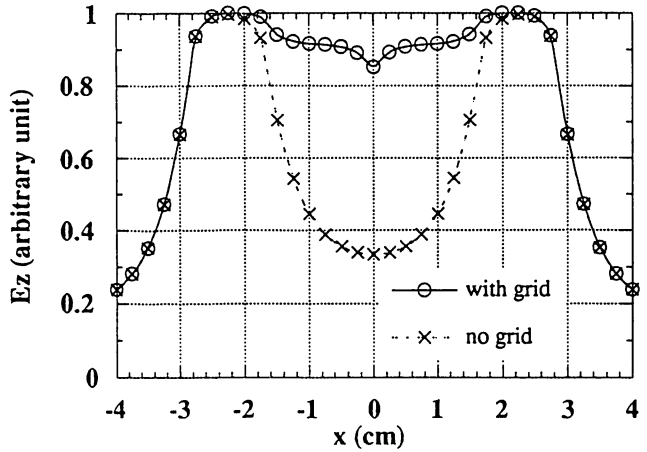

Fig. 9 Calculated electric fields in the xy-plane in the gap center. The circles indicate the fields with the grid-rings. The crosses indicate those without the grid-rings.

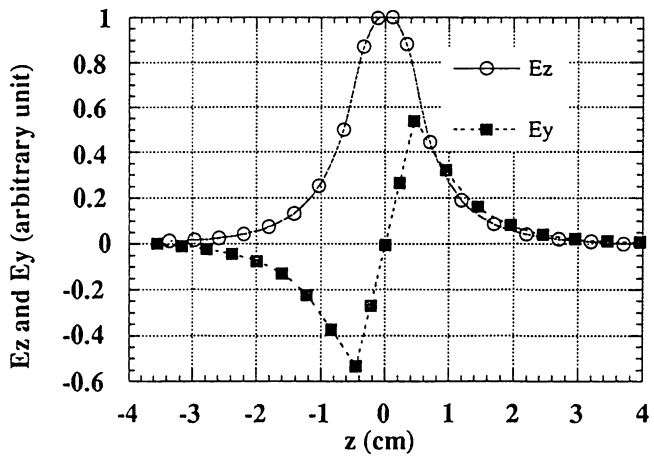

Fig. 10 Calculated electric fields (Ez and Ey components) along an axis separated from the z-axis by 12 mm for the no-grid-rings prebuncher.

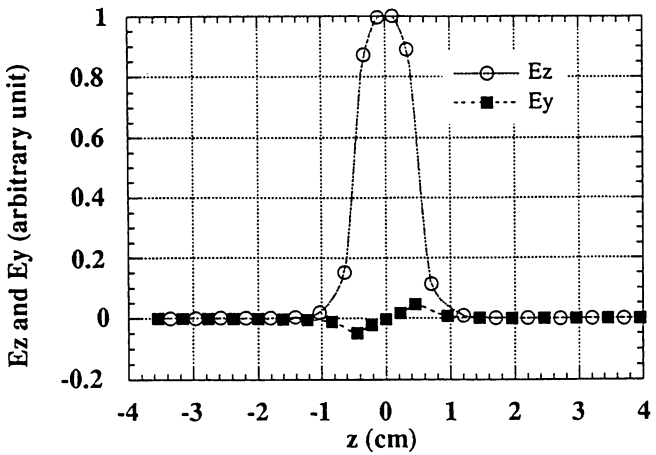

Fig. 11 Calculated electric fields (Ez and Ey components) along an axis separated from the z-axis by 12 mm for the grid-rings prebuncher.

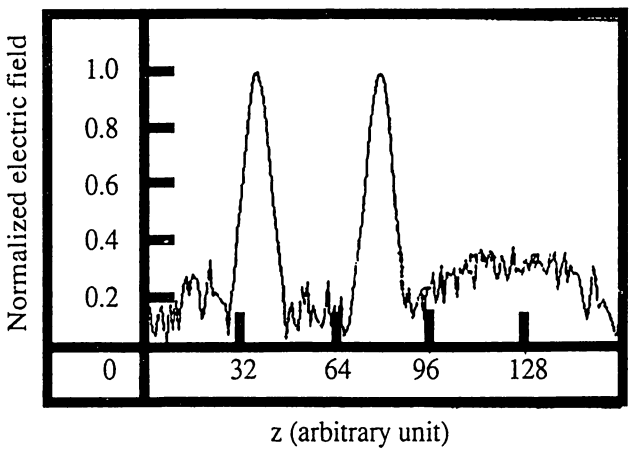

Fig. 12 Typical measured electric field along the z-axis for the no-grid-ring prebuncher.

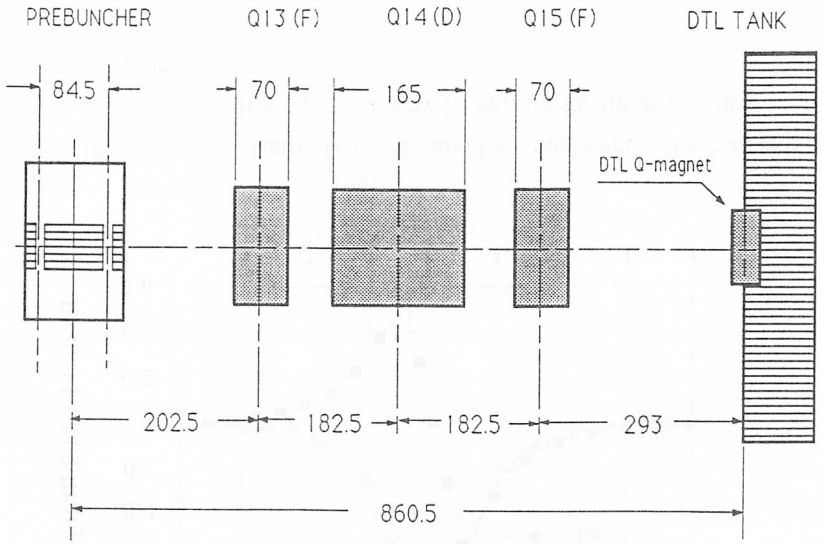

Fig. 13 Beam line between the prebuncher and the DTL.

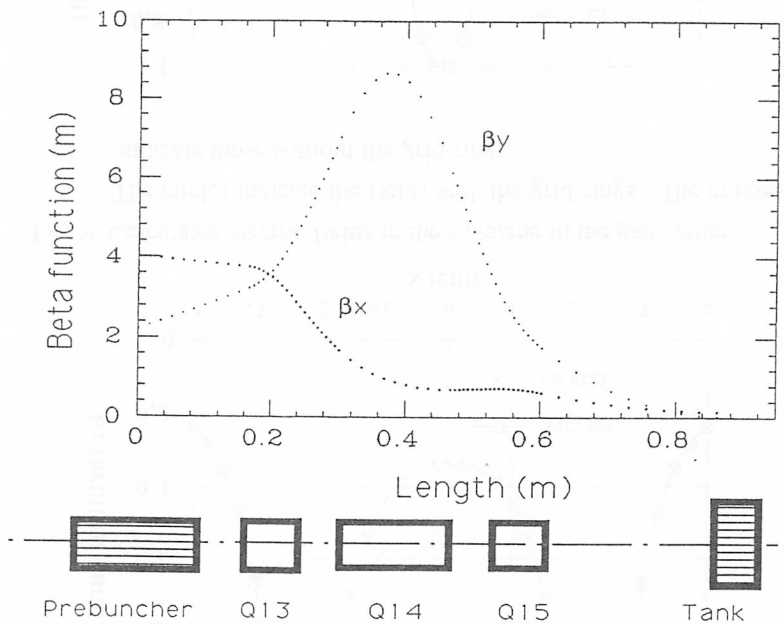

Fig. 14 β-functions of the beam line.

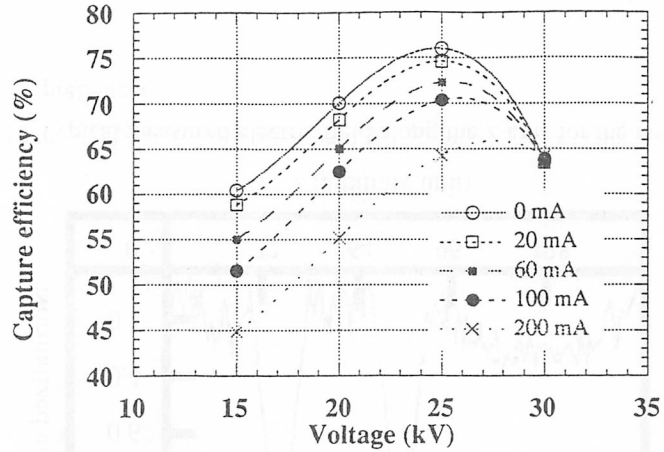

Fig. 15 Calculated capture efficiencies of the DTL for five kinds of currents. An rf stable angle of the DTL is assumed to be -26 degrees.

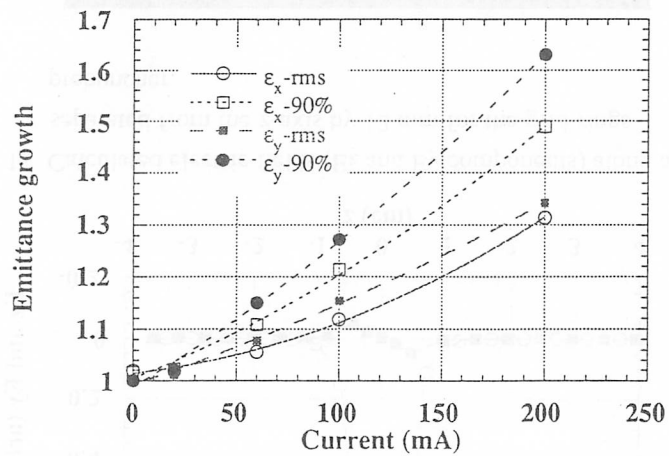

Fig. 16 Calculated emittance growth caused by the space-charge effects in the beam line. A normalized 90% emittance of 3πmm·mrad is assumed.

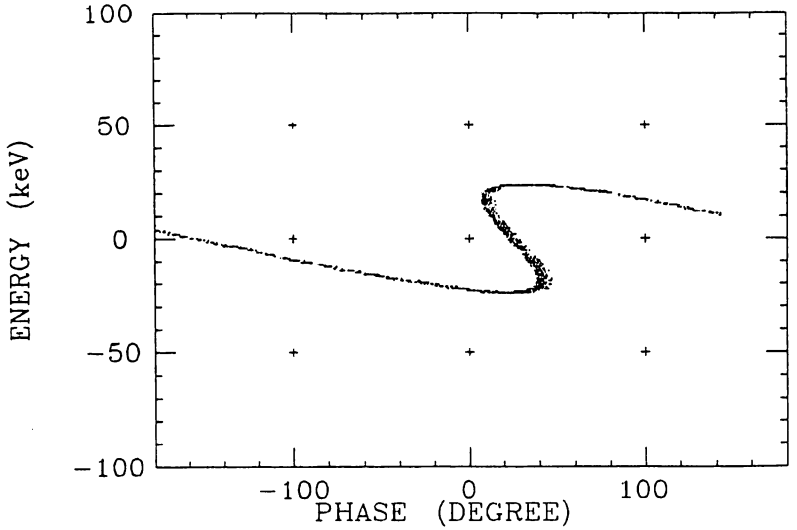

Fig. 17 Calculated longitudinal emittance for a zero-current beam at the DTL entrance. The prebuncher voltage is 25 kV.

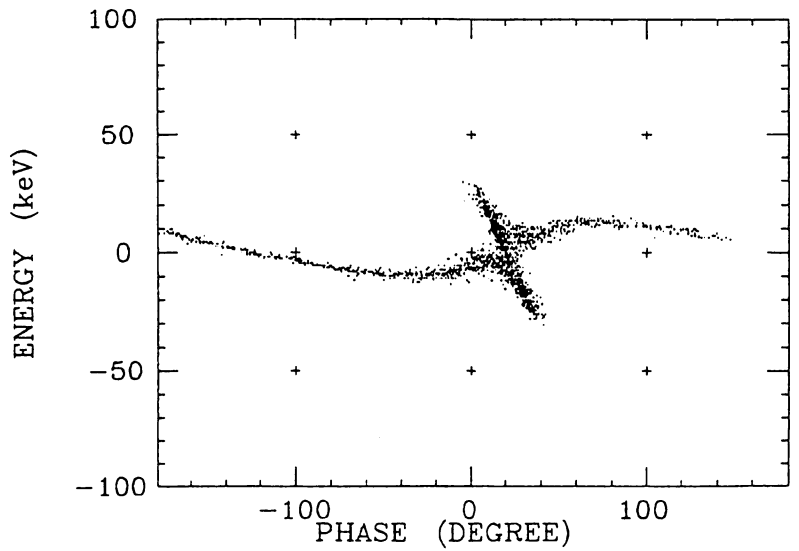

Fig. 18 Calculated longitudinal emittance for a 200-mA beam at the DTL entrance. The prebuncher voltage is 25 kV.

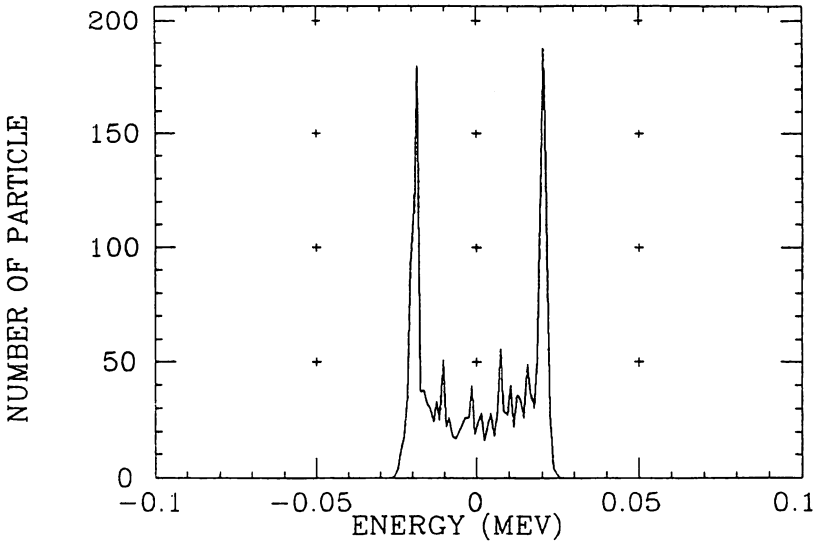

Fig. 19-1 Energy distribution for a 20-mA beam at the entrance of the DTL. The prebuncher voltage is 25 kV.

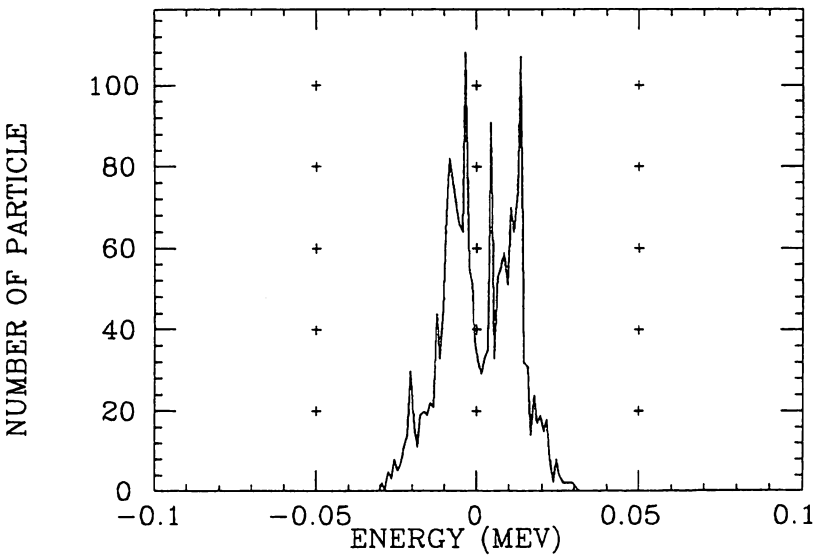

Fig. 19-2 Energy distribution for a 200-mA beam at the entrance of the DTL. The prebuncher voltage is 25 kV.

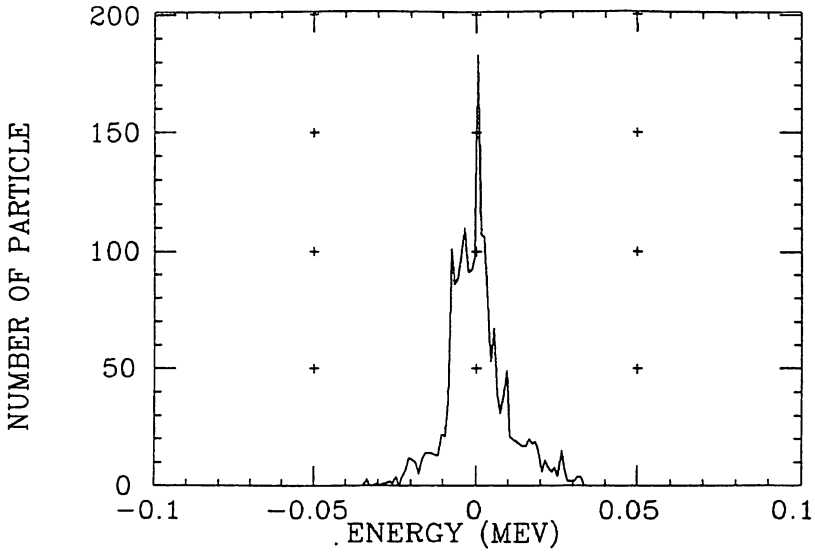

Fig. 19-3 Energy distribution for a 300-mA beam at the entrance of the DTL. The prebuncher voltage is 25 kV.

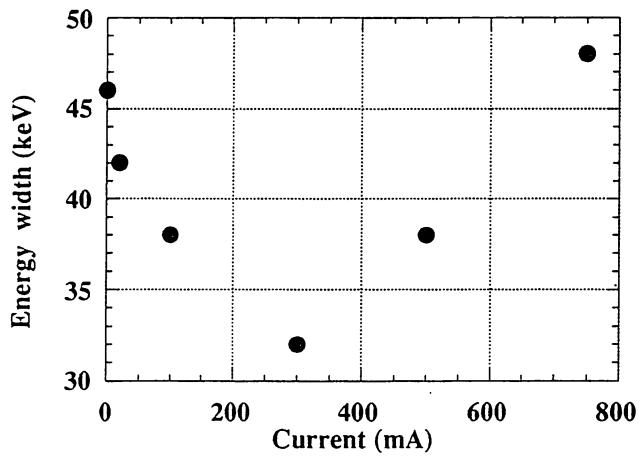

Fig. 20 Variation of the energy width (90%) versus current. The prebuncher voltage is 25 kV.

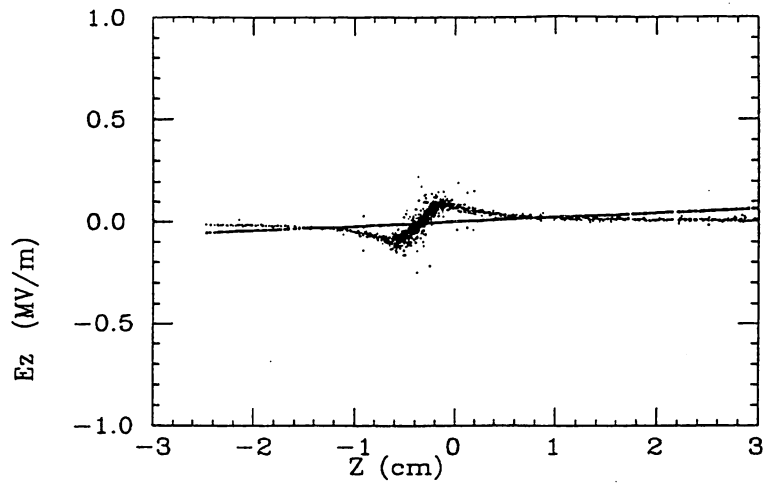

Fig. 21 Z-components of the electric field arising from space-charge (200 mA) at the DTL entrance. The dots indicate the results of the exact calculation for each particle. The inclined-line indicates the calculated values with a uniformly distributed equivalent ellipsoid.

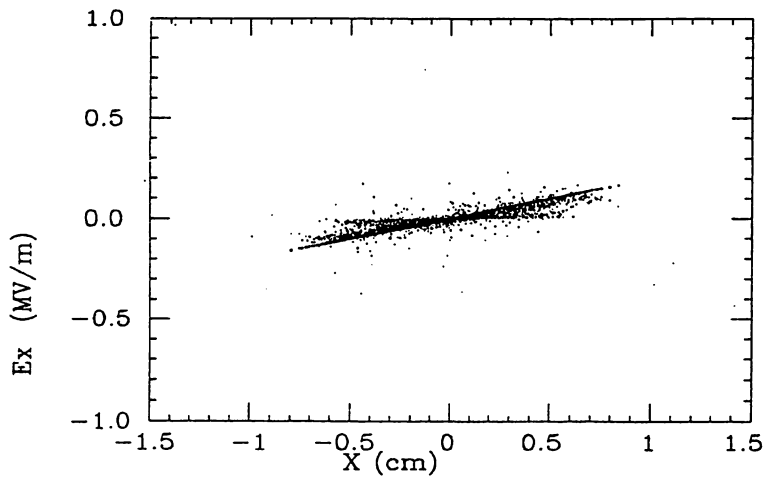

Fig. 22 X-components of the electric field arising from space-charge (200 mA) at the DTL entrance. The dots indicate the results of the exact calculation for each particle. The inclined-line indicates the calculated values with a uniformly distributed equivalent ellipsoid.

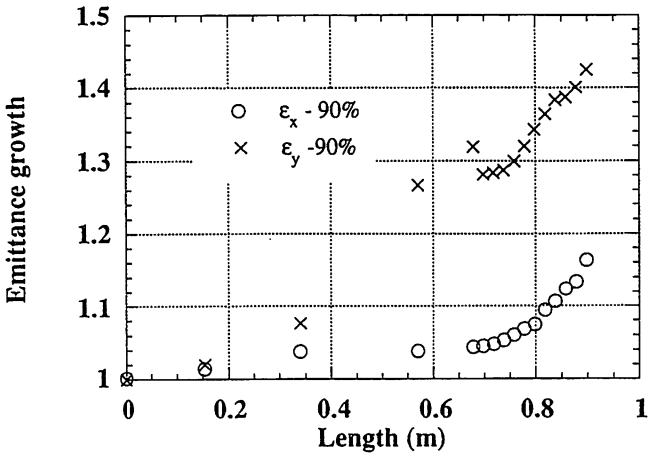

Fig. 23 Calculated emittance growth for a 200-mA beam with a normalized 90% emittance of 4πmm·mrad versus drift length after the prebuncher.